energies

MDPI

Article

Continuous Supercritical Water Impregnation Method for the Preparation of Metal Oxide on Activated Carbon Composite Materials

Florentina Maxim [1,*], Elena-Ecaterina Toma [1], Giuseppe-Stefan Stoian [1], Cristian Contescu [2,†], Irina Atkinson [1], Christian Ludwig [3,4] and Speranta Tanasescu [1]

[1] "Ilie Murgulescu" Institute of Physical Chemistry of the Romanian Academy, Splaiul Independentei 202, 060021 Bucharest, Romania; etoma@icf.ro (E.-E.T.); gstoian@icf.ro (G.-S.S.); irinaatkinson@yahoo.com (I.A.); stanasescu@icf.ro (S.T.)
[2] Oak Ridge National Laboratory, One Bethel Valley Road, Oak Ridge, TN 37831, USA; ccontescu@comcast.net
[3] Paul Scherrer Institute (PSI), ENE LEP CPM, 5232 Villigen PSI, Switzerland; christian.ludwig@psi.ch
[4] École Polytechnique Fédérale de Lausanne (EPFL), ENAC IIE GR-LUD, 1015 Lausanne, Switzerland
* Correspondence: fmaxim@icf.ro
† Retired.

Abstract: Metal oxide (Me_xO_y) nanomaterials are used as catalysts and/or sorbents in processes taking place in supercritical water (scH_2O), which is the "green" solvent needed to obtain energy-relevant products. Their properties are significantly influenced by the synthesis method used to prepare active Me_xO_y. In addition, the use of supported Me_xO_y nanoparticles is more practical and cost-effective in terms of their performance maintenance. Within this context, the present study reports on the preparation of carbon-supported ZnO and CuO composites using an innovative scH_2O impregnation method. Metal oxides were impregnated on a carbon (C) support using a continuous-flow tubular reactor. The results show that impregnation in scH_2O is a promising approach for the preparation of ZnO/C and CuO/C composite materials. This one-step synthesis method, in a continuous flow, uses neither a seed layer nor a mineralizer, and it needs substantially lower preparation times than conventional impregnation methods.

Keywords: supercritical water impregnation; continuous-flow tubular reactor; supercritical hydrothermal synthesis; metal oxide catalysts; metal oxide sorbents; carbon-based materials

Citation: Maxim, F.; Toma, E.-E.; Stoian, G.-S.; Contescu, C.; Atkinson, I.; Ludwig, C.; Tanasescu, S. Continuous Supercritical Water Impregnation Method for the Preparation of Metal Oxide on Activated Carbon Composite Materials. *Energies* **2024**, *17*, 913. https://doi.org/10.3390/en17040913

Academic Editor: Carlos Miguel Costa

Received: 10 November 2023
Revised: 31 January 2024
Accepted: 7 February 2024
Published: 16 February 2024

1. Introduction

A supercritical fluid is in a state above the critical temperature (T_{cr}) and critical pressure (p_{cr}) in the pressure–temperature phase diagram [1]. In the van der Waals theory of criticality, the critical point is the end of the liquid–gas equilibrium curve, the point at which liquid and gas reach the same density, which is the critical density (ρ_{cr}) [2]. For water, the corresponding values at the critical point are T_{cr} = 647 K, p_{cr} = 221 bar, and ρ_{cr} = 322 kg m^{-3}.

There has been vivid debate on whether there is a liquid–gas phase change associated with the fluid properties' variations in the region near the critical point, as no macroscopically visible interface between the liquid and gas appears in this region. Therefore, in textbooks, the supercritical state of a fluid is still presented as a homogeneous phase above the critical point [3]. However, since 2010, it has been demonstrated both theoretically and experimentally [4,5], and now, it is accepted that the supercritical state of a fluid can be divided into a gas-like (GL) region and a liquid-like (LL) regime by the transitional line, known as the Widom line [6–8], anticipating the phase separation and the coexistence that is found below the critical point [9].

The motivation behind our work is mainly related to the technological applications of scH_2O. For instance, water and wastewater treatments can be performed via oxidation in

scH_2O [10], and gas fuels, such as H_2 or CH_4, can be obtained from wet biomass by gasification [11]. The main advantage of scH_2O technologies is their efficiency, which resides in the fact that the complete conversion or total removal of organic pollutants is achieved very quickly, sometimes after only a few minutes [12]. Moreover, using scH_2O, technically difficult feedstocks can be treated effectively, with high selectivity for valuable compounds, while the reaction's products are harmless [13]. In addition, catalytic supercritical water gasification technology is highly energy-efficient. High thermal process efficiency in the conversion of biomass to synthetic natural gas (SNG) of 60–70% (typical) and beyond 70% for the poly-generation of SNG, electricity, and heat is possible [14]. However, the disadvantages of scH_2O technologies are the high operation costs resulting from high-temperature and high-pressure working conditions and the associated issues related to salt deposition. A solution to these problems could be the use of functional materials [15], such as catalysts, that could decrease the process temperature and lead to energy savings. Sorbent materials can adsorb heteroatoms, such as sulfur or chlorine, which helps to overcome issues related to salt precipitation and catalyst poisoning. Metal oxides are good candidates as catalysts or sorbents in scH_2O [15,16]. Their functional properties, such as their activity, selectivity, and stability under supercritical conditions, might be greatly affected by the synthesis method. Among the various preparation methods, hydrothermal synthesis in scH_2O has the following advantages: high reaction rates, the one-step production of well-defined Me_xO_y with controlled size and shape, and reduced alkaline concentration for crystal growth [17,18]. In addition, running hydrothermal synthesis in a flow reaction system is more advantageous than using batch reactors due to the possibility of including engineered mixers for the scH_2O and the metal salt precursors [19]. Moreover, in flow reaction systems, the density of water can be varied by controlling the temperature and pressure during the reaction. Thus, the desired shape/morphology of the Me_xO_y nanoparticles can be achieved. For instance, at a relatively higher water density, ZnO particles with 1D morphology can be obtained, whereas at a low water density, mostly spherical-like nanoparticles are formed [17]. The characteristics of active Me_xO_y, such as particle size, morphology, and structure, influence the catalytic and sorption properties of the composite material. As an example, ZnO tetrapods exhibit enhanced adsorption properties for hexavalent chromium from aqueous solutions [20], whereas spherical ZnO particles exhibit good antibacterial and photocatalytic activities [21]. In addition, nanowires of CuO with a monoclinic structure and an average crystallite size of ~17 nm are employed for the removal of methylene blues from an aqueous solution [22].

Considering that it is very important to maintain the performance of metal oxides as catalysts or sorbents under scH_2O conditions, it is efficient and cost-effective to use supported Me_xO_y nanoparticles, with the advantages of enhanced mechanical and thermal stability and facile regeneration and reuse. The usual procedure for the preparation of composite materials is impregnation, followed by drying to obtain the final composite. The loading (amount of metal oxide that determines its efficiency) on the support and the dispersion (concentration profile) within the support pores depend significantly on the impregnation and drying conditions [23]. The porous carbon materials used as supports may also influence the formulation of the composites in terms of dispersion and loading due to different surface chemistry and transport properties through the pores. It has been reported that the degree of carbon surface oxidation has a strong influence on the distribution of the metal precursor on the support [24], whereas the use of carbon nanotubes as supports allows for the homogenous growth of ZnO nanowires [25] and the transportation of small nanoparticles through the nanochannels due to increased fluidity [26]. It is important to note that by conventional impregnation methods, such as wet impregnation and pore volume impregnation [27], the redistribution of active metal oxides can occur during the drying stage, which in turn lowers the catalytic/sorption capacity. The supercritical water impregnation method in a batch reactor was developed in order to obtain highly dispersed metal oxides on porous supports [28]. Moreover, the method simplifies the process of impregnation due to the fact that post-treatments, such as calcining and drying,

are not needed [29], and therefore, the agglomeration and/or the redistribution of the active nanoparticles within the support is avoided.

The present work is focused on the development of a continuous-flow supercritical water impregnation method for the preparation of zinc oxide and copper oxide nanoparticles on carbon support, which are composite materials with specific functionalities for separation processes in scH_2O.

2. Materials and Methods

$Zn(NO_3)_2 \cdot 6H_2O$ p.a. crystallized, ≥99.0%, and $Cu(NO_3)_2 \cdot 3H_2O$ p.a. 99–104% from Sigma Aldrich were used as precursors. Aqueous solutions with different concentrations, namely, 0.0041 M, 0.0082 M, and 0.0164 M, were prepared in ultrapure, degassed water. Porous materials based on carbon were used as a support for the impregnation of the metal oxides. The carbonaceous porous materials have a graphitic, monolithic structure and are composed of activated carbon fibers with an average diameter in the micrometric scale (10–20 μm) [7]. The support has the following characteristics: a specific surface area of approx. 1100 $m^2\ g^{-1}$ and a total pore volume of approx. 0.6 $cm^3\ g^{-1}$, as measured via N_2 adsorption at 77 K, and a water absorption capacity of 165%.

Metal oxides were impregnated using the continuous-flow tubular reactor of the NISA equipment (Neutron Imaging Supercritical-water Analysis) described in [7]. The main component of NISA was the continuous-flow tubular reactor, equipped with an embedded preheater, and an aluminum block heater. The fluid was fed into the reactor in the upward direction using high-pressure liquid chromatography pumps. In the setup, the pressure was built and controlled using a back pressure regulator. The operating parameters, such as temperature, pressure, water flow rate, and mass balance, were controlled and monitored online, and the values were recorded every 10 s [7]. Three synthesis parameters were studied to understand their influence on the composite's formulation in terms of crystallinity, size, and morphology, as well as the loading and concentration profile of the active element on the support. These were (i) the impregnation temperature chosen to provide scH_2O densities corresponding either to LL or to GL phases of water [8], (ii) the flow rate determining both the residence time and the contact time between the metal precursor solution and the C support surface, and (iii) the concentration of the metal nitrate aqueous solution used as the precursor.

Each experimental run started by loading the reactor with ~0.2 g of carbon support, followed by filling the system with water, preheating at 573 K, and application of a constant pressure of 250 bar to reach supercritical conditions. When the water inside the reactor reached the temperature of interest for impregnation, metal precursor solution was fed in at flow rates of 2.5 mL min^{-1}, 5 mL $min^{-1,}$ or 7.5 mL min^{-1}, corresponding to flow velocities of 3.7×10^{-4} m s^{-1}, 7.4×10^{-4} m s^{-1}, and 11.0×10^{-4} m s^{-1}, respectively. The impregnation was performed under steady-state conditions for 1 h. The mass of the metal precursor solution was recorded for each experiment, and the amount of metal available for deposition on the carbon support was calculated in this manner. The impregnation temperature was either 648 K or 668 K. These temperatures were chosen to be 10 K lower and higher, respectively, than the transition temperature between the LL and GL phases of scH_2O at a pressure of 250 bar [8]. The sample index contained the starting metal ion/the molar concentration of the aqueous nitrate solution (mol L^{-1}), the fluid flow rate (mL min^{-1}), and the synthesis temperature (K). For example, the sample obtained from 0.0041 M zinc nitrate at 5 mL min^{-1} flow rate and 668 K was indexed as Zn^{2+}/0.0041 M/5 mL min^{-1}/668 K.

The crystallographic structure of the as-prepared composite materials was analyzed by X-ray diffraction (XRD) using a Rigaku's Ultima IV diffractometer in parallel beam geometry, with Cu Kα radiation (λ = 1.5406 Å), and operated at 40 kV and 30 mA. The signals were collected from 10° to 80° with a step size of 0.02°, and a scan speed of 2° min^{-1}. The identification of the present phases was performed using Rigaku's PDXL software,

connected to the ICDD PDF-2 database. The crystallite size was calculated using the Scherrer equation:

$$D = \frac{k\lambda}{\beta \cos\Theta} \quad (1)$$

where λ is the wavelength of the CuKα radiation (1.54056 Å); β, FWHM of the diffraction peak; θ, diffraction angle; and k, constant.

Other structural information was obtained via room-temperature infrared spectroscopy (FTIR) using a NICOLET IS10 spectrometer (Thermo Fisher, Eindhoven, The Netherlands) equipped with a total attenuated reflection module. The measurements were performed using scans between 500 and 4000 cm^{-1}. The peak locations and intensities were determined using the Omnic software (Nicolet Instrumentations Inc., Madison, WI, USA).

The morphological analysis was performed by scanning electron microscopy (SEM) with an FEI Quanta 3D FEG microscope operated at 5 kV acceleration voltage. The transmission electron microscopy (TEM) characterization of the composite materials was performed using a Hitachi HD-2700 Scanning Transmission Electron Microscope (STEM) at 200 kV accelerating voltage with a crystal lattice resolution of 0.144 nm under ideal conditions (Hitachi High-Technologies Corporation, Ibaraki, Japan). Chemical composition analysis was performed with the same equipment using an EDS short-time elemental mapping module. For the TEM analysis, the samples obtained by impregnation under scH_2O conditions were crushed and dispersed in ethanol. A drop of the resulting suspension was then deposited on a Cu grid containing a holey carbon thin film.

3. Results

3.1. Effect of the Impregnation Temperature

Figure 1 presents the XRD patterns of the samples obtained from the Zn^{2+} and Cu^{2+} precursors at two different impregnation temperatures, 648 K and 668 K, respectively. The XRD analysis revealed that ZnO with a hexagonal structure was formed at both temperatures (Figure 1a). It is important to note that the ZnO XRD peak intensities decreased as the reaction temperature increased. This is different when starting from Cu precursor, where the formation of copper oxides was revealed by XRD only at impregnation temperatures above the Widom line (668 K).

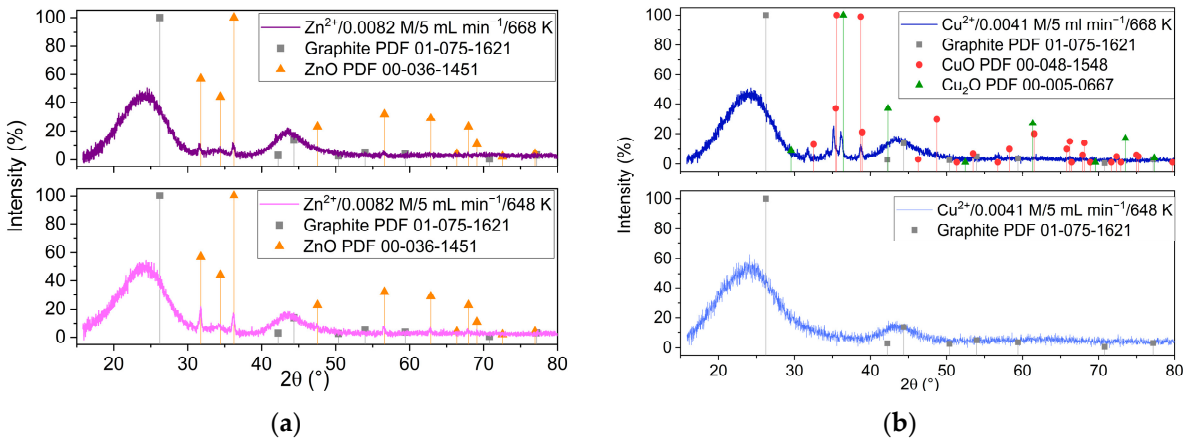

Figure 1. XRD patterns of the samples obtained at two different impregnation temperatures, starting from (**a**) zinc and (**b**) copper precursors.

Figure 2 shows the FTIR spectra of the ZnO/C and CuO/C type composite materials obtained at 668 K and, for comparison, the spectrum of the initial carbon support. The three spectra were similar at wave numbers of up to 1200 cm^{-1}. The spectral bands observed in the region of 3600–3100 cm^{-1} were attributed to the O-H bonds in the water molecule. Also, the OH groups were confirmed by discrete absorption bands around 1387–1405 cm^{-1} [30]. The bands in the 2600–1900 cm^{-1} region correspond to the C=C

stretching vibrations of numerous sp^2 structures that enrich the carbon structure [31]. The presence of C=O bonds was indicated by the spectral bands in the 1500–1400 cm^{-1} range. The bands specific to metal–oxygen bonds were observed in the fingerprint region between 1200 and 700 cm^{-1} [32]. Moreover, the characteristic bands of the Cu-O bonds were observed in the region of 550–600 cm^{-1} [33,34].

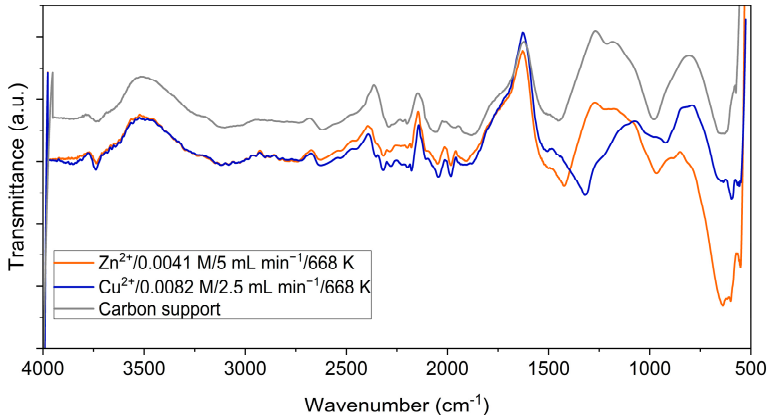

Figure 2. FTIR spectra of ZnO/C and CuO/C composite materials; the spectrum of the carbon support is presented for comparison.

We analyzed the effect of the impregnation temperature by SEM, and the results are presented in Figure 3. Note that, starting from either Zn^{2+} or Cu^{2+} precursors, Me_xO_y particles with 1D rod-like morphology and diameter within the µm scale were formed at 648 K; these types of particles appeared to form separately from the carbon fiber surface (Figure 3a–d). The SEM analysis of the samples obtained at an impregnation temperature of 668 K (Figure 3e–h) revealed carbon fibers covered by Me_xO_y nanoparticles on the surface along with isolated regions containing the 1D Me_xO_y particles. Based on this observation, the impregnation/deposition of metal oxide structures on the carbon surface was further performed at this temperature.

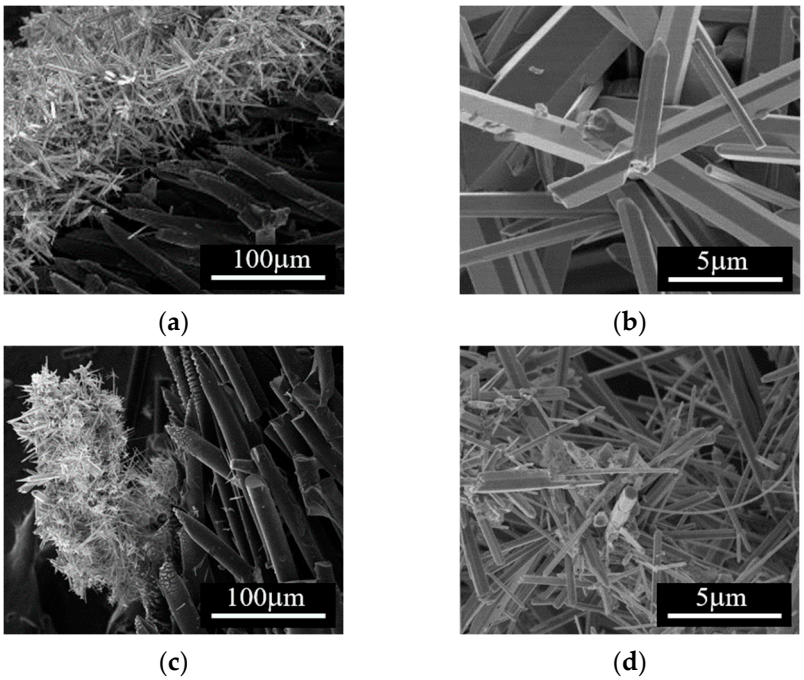

Figure 3. *Cont.*

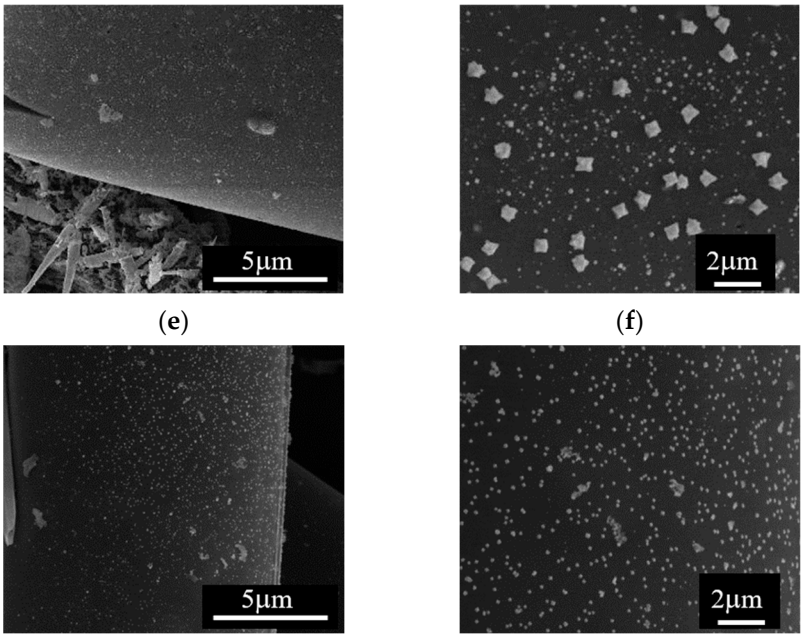

(**e**) (**f**) (**g**) (**h**)

Figure 3. SEM images of the samples obtained at different impregnation temperatures: (**a**–**d**) at 648 K; (**e**–**h**) at 668 K, starting from (**a**,**b**,**e**) and (**f**) Zn^{2+} and (**c**,**d**,**g**), and (**h**) Cu^{2+} precursors; right-side SEM images show higher magnification of the images presented on the left side.

Figure 4 shows the results of TEM characterization and chemical composition analysis by EDS for the ZnO/C type material obtained at 668 K, with a 5 mL min^{-1} flow rate and 0.0041 M zinc concentration in the precursor solution. The TEM images (Figure 4a,b) reveal the formation of small crystalline particles of approx. 50 nm in size, and the EDS maps presented in Figure 4c–f confirm that these nanoparticles are ZnO on C support.

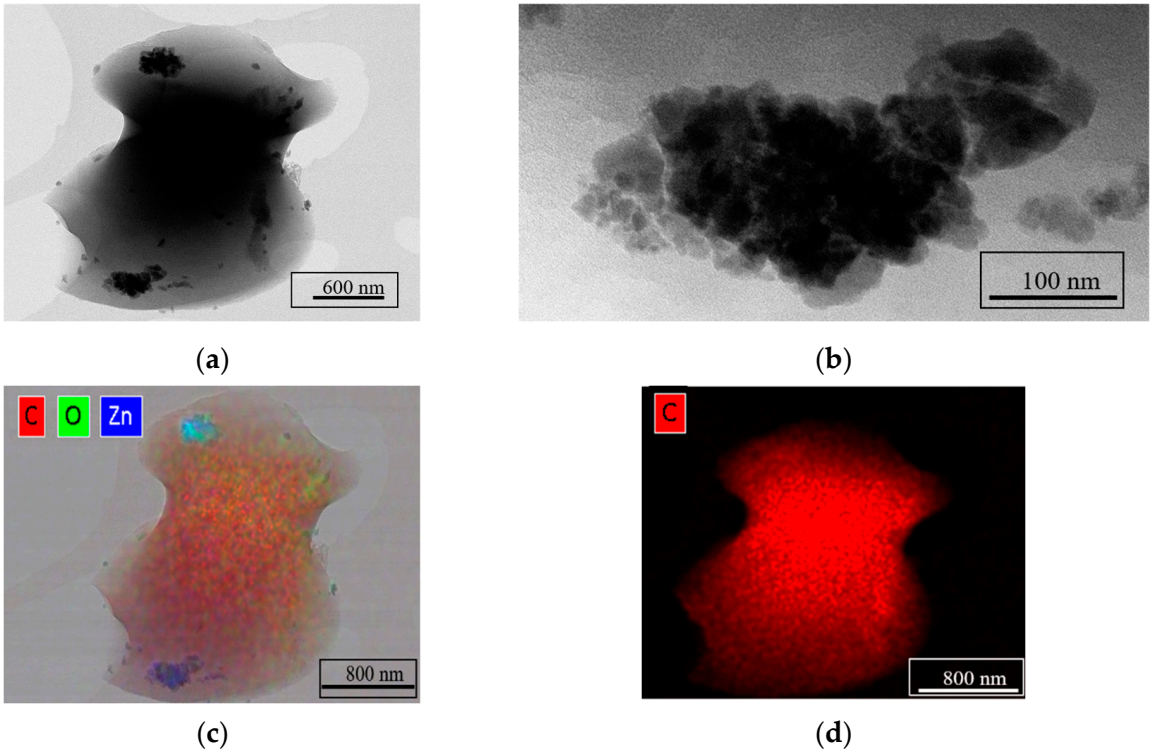

(**a**) (**b**) (**c**) (**d**)

Figure 4. *Cont.*

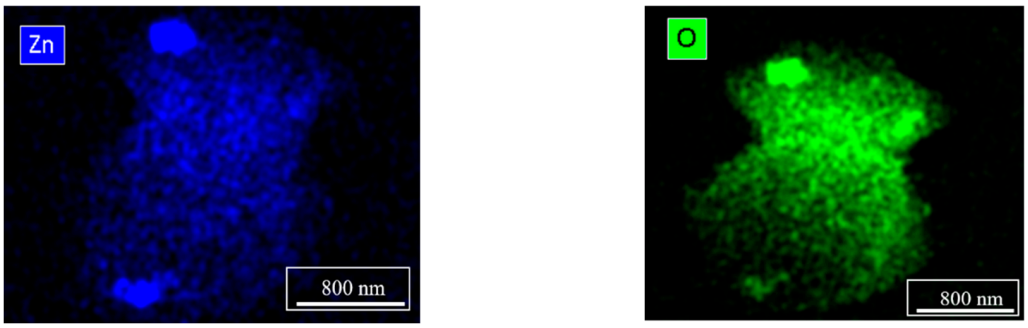

(**e**) (**f**)

Figure 4. TEM characterization of the sample Zn^{2+}/0.0041 M/5 mL min^{-1}/668 K: (**a**,**b**) STEM images; (**c**–**f**) the EDS maps confirming the formation of ZnO nanoparticles on C support.

3.2. Effect of the Fluid Flow Rate

Figure 5 presents the XRD analysis of the samples obtained from Zn^{2+} (Figure 5a) and Cu^{2+} (Figure 5b) precursors with two different flow rates of the reactant mixture during impregnation (2.5 mL min^{-1} and 5mL min^{-1}, respectively). It should be noted that increasing the flow rate allowed the formation of more crystalline ZnO (Figure 5a) and the formation of CuO (Figure 5b). At a low flow rate instead, Cu_2O was predominately formed, indicating the influence of the redox environment related to the higher rate of mixing.

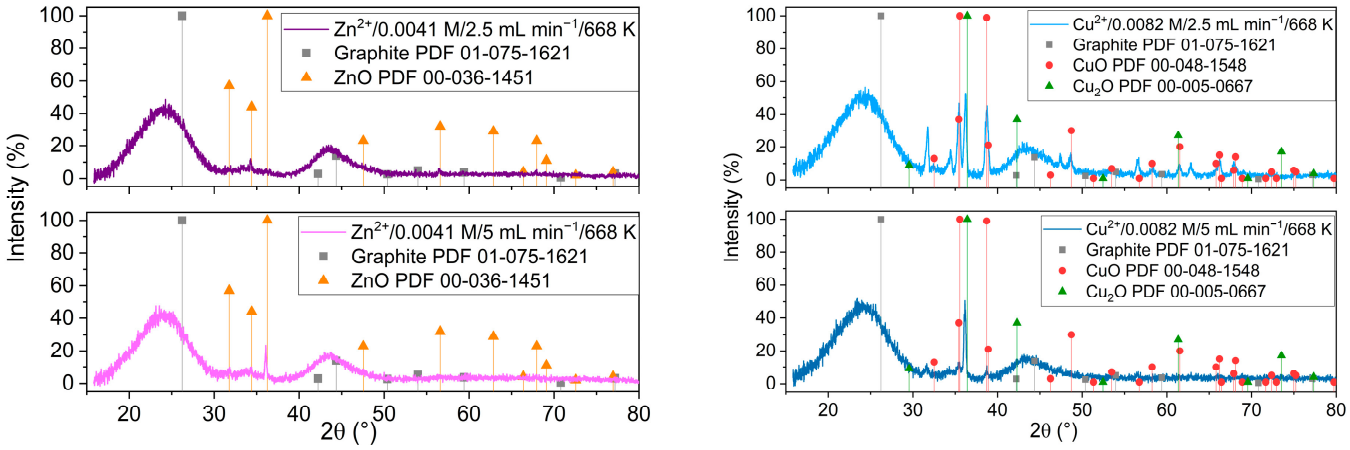

(**a**) (**b**)

Figure 5. XRD patterns of the samples obtained at 668 K, different flow rates, and starting from (**a**) Zn^{2+} and (**b**) Cu^{2+} precursors.

The effect of the flow rate on the impregnation procedure is more evident in the SEM analysis of ZnO/C composite materials presented in Figure 6. There were 1D particles attached to the carbon fibers at both flow rates (Figure 6a,b,e,f); however, at a low flow rate, the surface of the carbon fibers was covered by hexagonal-shaped nanoparticles of different sizes (Figure 6c,d), whereas at a higher flow rate, there were carbon fibers homogeneously covered with Me_xO_y crystalline cuboid-shaped nanoparticles of about 60 nm in size (Figure 6g,h).

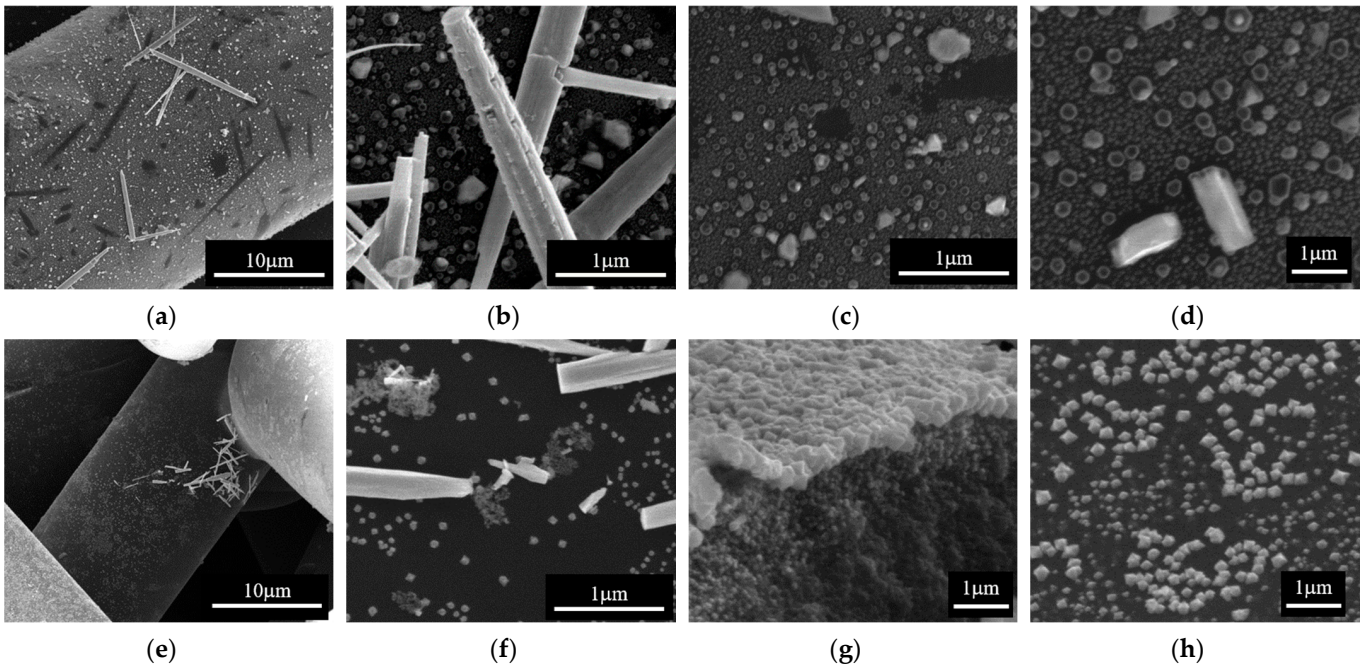

Figure 6. SEM analysis of the ZnO/C samples obtained starting from [Zn^{2+}] = 0.0041 M by impregnation at 668 K and two different flow rates of the reactant mixture: (**a**–**d**) at 2.5 mL min^{-1}; (**e**–**h**) at 5 mL min^{-1}.

3.3. Effect of the Metal Ions Concentration in the Aqueous Precursor Solution

The XRD patterns of the ZnO/C composite materials obtained using different concentrations of the precursor solution are presented in Figure 7a. Note that hexagonal ZnO structures were formed at all initial Zn^{2+} concentrations, whereas high-crystallinity ZnO was obtained only by increasing the starting amount of zinc ions (inset in Figure 7a). The XRD results of the samples obtained from the Cu^{2+} precursor, with different initial concentrations, are presented in Figure 7b. An important observation from the analysis of the XRD patterns of these samples was that decreasing the Cu^{2+} concentration might promote the formation of CuO. However, the inset in Figure 7b shows that the corresponding diffraction peaks of the Cu_2O structure shifted towards lower 2θ angles compared to the reference. Moreover, unidentified diffraction peaks were observed in the XRD patterns of these samples. Surprisingly, no copper oxide formation at high concentrations was revealed by XRD.

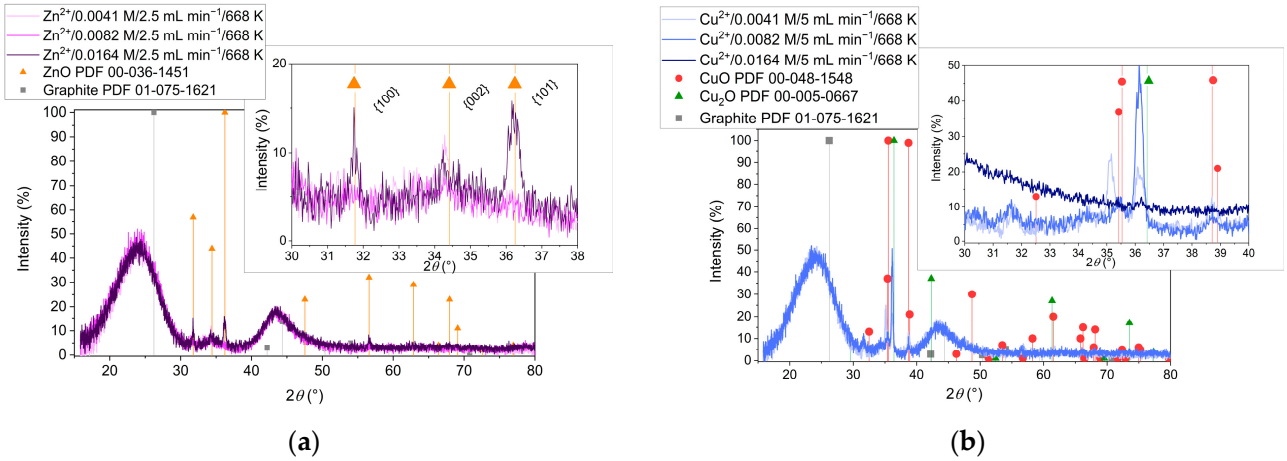

Figure 7. XRD patterns of the samples obtained from (**a**) Zn^{2+} and (**b**) Cu^{2+} with different metal ion concentrations in the precursor solutions.

By SEM, the effect of the initial cation concentration on the impregnation of Me_xO_y was more evident for the ZnO/C-type samples, as presented in Figure 8. First, zinc oxide nanoparticles were deposited on the surface of the carbon fibers at all starting concentrations of Zn^{2+} in the precursor solution (Figure 8a,d,f). Second, at low concentrations, we noticed that ZnO covered the carbon fibers more homogeneously, whereas increasing the Zn concentration led to an increase in the particles' dimensions from around 60 nm (Figure 8b) to 80 nm (Figure 8e), and finally to over 200 nm (Figure 8g). Finally, a flower-like morphology of the ZnO nanoparticles was observed (Figure 8c,h).

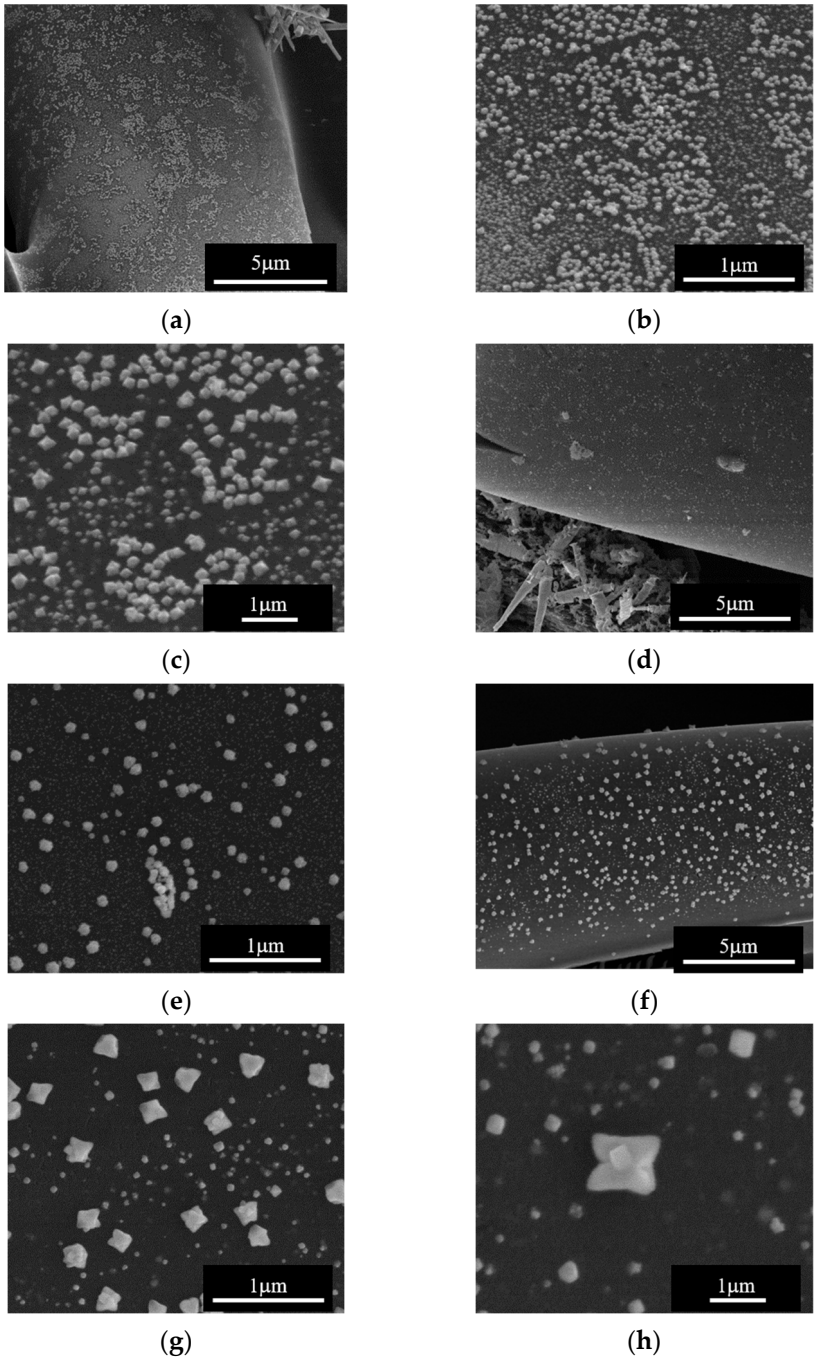

Figure 8. SEM images of samples obtained at different concentrations of Zn^{2+} in the precursor solution: (**a**–**c**) for Zn^{2+}/0.0041 M/5 mL min^{-1}/668 K; (**d**,**e**) for Zn^{2+}/0.0082 M/5 mL min^{-1}/668 K; (**f**–**h**) for Zn^{2+}/0.0164 M/5 mL min^{-1}/668 K.

The SEM analysis of the sample obtained at 668 K with a low Cu^{2+} concentration and low flow rate of the precursor solution showed the formation of large 1D particles together with nanoparticles uniformly covering large areas of the carbon surface. Figure 9 presents this result and shows the morphological details at different magnifications of the copper oxide nanoparticles formed under the above-mentioned conditions.

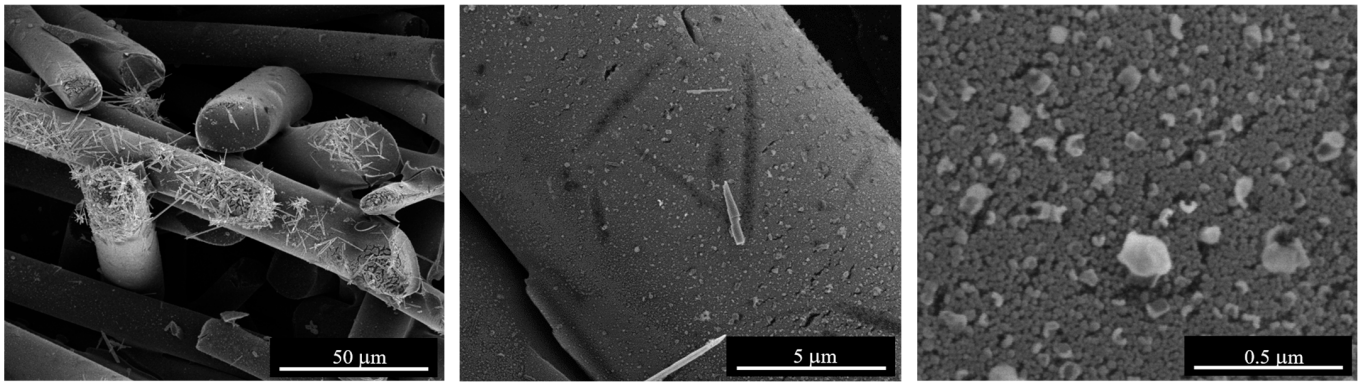

(**a**) (**b**) (**c**)

Figure 9. SEM analysis of sample Cu^{2+}/0.0041 M/2.5 mL min^{-1}/668 K showing microstructural and morphological details of the surface of the CuO/C composite material; (**a**–**c**) are the SEM images of the same sample acquired at different magnifications.

4. Discussion

The results presented above show that zinc oxide and copper oxides are formed under scH_2O conditions and that the 668 K impregnation temperature is optimum for the deposition of Me_xO_y nanoparticles on the carbon fiber support (Figures 1–4). This temperature and low flow rates of the metal precursor solution favor the formation of CuO (Figure 5), whereas the high flow rate of the Zn^{2+} solution allows the homogenous deposition of ZnO nanoparticles on the surface of the carbon fibers (Figure 6). The metal ion concentration in the starting solution does not have a significant influence on the formation of Me_xO_y structures (Figure 7). However, increasing the Zn^{2+} concentration resulted in an increase in the size of the flower-like ZnO nanoparticles impregnated on the carbon fibers (Figure 8). Instead, the copper oxide nanoparticles are more homogeneously impregnated on the support fibers at low concentrations of Cu^{2+} in the precursor solution (Figure 9). It should be noted that ZnO, CuO, and Cu_2O phases formed under the supercritical conditions of this study have an average crystallite size of 25 nm, 26 nm, and 30 nm, respectively.

The related hydrothermal reactions leading to the formation of metal oxides from nitrates correspond to the hydrolysis of metal ions and dehydration of the corresponding hydroxides, according to the reactions below:

$$\text{Hydrolysis: } Me(NO_3)_x + xH_2O \rightarrow Me(OH)_x + xHNO_3 \quad (2)$$

$$\text{Dehydration: } Me(OH)_x \rightarrow MeO_{x/2} + x/2\ H_2O \quad (3)$$

In this homogeneous phase mechanism, water acts as both a reactant and solvent, and its property variation, like density and dielectric constant, significantly affects the rate of these reactions [18].

Based on neutron imaging measurements, Maxim et al. obtained a water phase diagram in the supercritical region and confirmed the position of the Widom line that separates the LL and GL regimes of scH_2O [8]. At 250 bar, the water temperature of 648 K corresponds to the LL densities with values around 500 kg m^{-3}, whereas at 668 K, water is in the GL state, with a density of around 150 kg m^{-3}. Moreover, the dielectric constant of water drops from values around 10 to below 5 when the temperature is increased across the Widom line [35]. The water property variation explains the effect of the synthesis

temperature on the formation of Me_xO_y during impregnation on C fibers. It is known that, on increasing the temperature under supercritical conditions, the hydrolysis rate of metal salt precursors substantially increases with a decrease in the water dielectric constant, while the dehydration equilibrium shifts towards oxides [18]. This is also in agreement with a study by Ludwig and Casey [36], who concluded that hydrolyzed cations are more reactive than non-hydrolyzed cations. Hydrolyzed species may, therefore, favor the formation of Me_xO_y structures and act as relevant precursors under scH_2O conditions, as presented in this study. However, further studies are needed to elucidate the details of the Me_xO_y formation mechanism under scH_2O conditions.

Interestingly, the deposition of Me_xO_y nanoparticles on the carbon fibers was observed only at synthesis temperatures corresponding to the GL phase of scH_2O. When water was in the LL phase, only the formation of 1D Me_xO_y particles attached to the support fibers was noticed. It has been reported that, during scH_2O impregnation on porous activated carbon supports, two mechanisms of particle deposition are possible. The first route is related to the particles formed in the bulk phase, followed by adsorption to the support surfaces; in the second scheme, the nanoparticles are formed at the support surfaces followed by particle growth [37]. Our results indicate that both mechanisms of impregnation occur, and the ratio between the number of particles formed in the bulk and those formed at the carbon surface depends on the variation in both scH_2O transport and solvent properties with the impregnation temperature. In the GL phase, the dielectric constant of scH_2O is two times lower than that in the LL state. Consequently, the metal salt hydrolysis reaction rate increases substantially, and the formation of nitric acid is faster under GL conditions than in the LL regime. Surface carbon oxidation by NO_3^- ions may initiate a second heterogeneous mechanism for copper oxide deposition. Oxidation introduces oxygen-containing surface groups, (carboxyls and phenols) which increase the hydrophilic character of the carbon surface and likely enhance the adsorption of hydrated cations [38]. Both carboxylic and phenolic groups act as ligands for Cu^{2+} and Zn^{2+} ions and may displace water from the aqueous ion [39]. The higher difficulty of obtaining copper oxides compared with the zinc oxide reported above may originate from the higher stability of copper complexes with oxygenated functional groups on the carbon surface. Indeed, Cu^{2+} (d^9) complexes on the carbon surface should be more stable than Zn^{2+} (d^{10}) analogs [40,41] for reasons that depend on ion size differences and a possible Jahn–Teller symmetry deformation only for Cu^{2+}.

The in situ neutron imaging measurements reported by Maxim et al. [7] help to understand that the carbon monolith used as a support for impregnation acts as a static mixer [42], which allows the visualization of different hydrodynamic regimes inside the monolith in the neutron radiography of the scH_2O reactor [7]. In addition, it is reported in our previous work that there are two pore sizes to consider in the carbon support: micropores within the fibers and macropores forming interfibrillar voids [7]. Therefore, it is expected that the reactant mixture flow rate influences the mixing efficiency within the monolith support and the residence time of the metal precursors on the fibers' surface. To obtain well-defined Me_xO_y nanoparticles in terms of size, morphology, and structure, the mixing rate of scH_2O with the metal precursor solution should be high compared to the formation reaction rate [43,44]. Zinc and copper oxides are formed under the studied scH_2O conditions independent of the flow rate. However, the SEM analysis confirmed that there is a difference in the nucleation and growth mechanism when changing the flow rate. Increasing the Reynolds number and decreasing the mixer dimension lead to an increase in both the nucleation rate and growth rate because efficient mixing results in higher supersaturation [45].

The concentration of the metal ions in the precursor solution might influence the growth direction and the aspect ratio of the Me_xO_y nanoparticles; these results are in agreement with previous reports, especially for the ZnO synthesis in scH_2O [46,47]. Further optimization of the impregnation conditions is planned for future studies. It is known that the amount, distribution, and size/morphology of Me_xO_y nanoparticles deposited on

carbon supports are influenced by the pH of the reaction mixture [47,48]. Another working condition to be optimized is the impregnation time. It has been reported that this parameter may influence the pore volume and the surface area of composite materials obtained via supercritical water impregnation [28,29].

5. Conclusions

Under isobaric supercritical conditions, increasing the synthesis temperature to the values at which scH_2O is in the GL phase favors the impregnation of metal oxides on activated carbon fiber monolithic supports. The uniform impregnation of support fibers with ZnO crystalline nanoparticles of hexagonal symmetry, cubic morphology, and ~60 nm in size was obtained at 250 bar and a reaction temperature of 668 K. Under the same temperature and pressure conditions, the impregnation of CuO on the same type of support is favored when starting from low concentrations of Cu^{2+} in the aqueous precursor solution and at low flow rates of the precursor solution through the reactor. These conditions determine the contact time between the metal precursor and the surface of the carbon support. The crystalline nanoparticles of cupric oxide, of monoclinic symmetry and cubic morphology, with dimensions of 50 nm, uniformly cover the carbon fibers.

The results show that hydrothermal impregnation in scH_2O is a promising method for the preparation of Me_xO_y/C composite materials in continuous flow. The method described here has the advantage that it can be performed in a single synthesis step, without a seed layer and a mineralizer, and at substantially lower preparation times than conventional impregnation methods.

Author Contributions: Conceptualization, F.M.; methodology, F.M., E.-E.T. and G.-S.S.; data curation, E.-E.T., G.-S.S. and I.A.; writing—original draft preparation, F.M., C.C. and C.L.; writing—review and editing, F.M., C.C., C.L. and S.T. All authors have read and agreed to the published version of the manuscript.

Funding: This work was supported by a grant from the Romanian Ministry of Research, Innovation, and Digitization, CNCS/CCCDI—UEFISCDI, project number PN-III-P4-ID-PCE-2020-1241 (acronym APASUPER), within PNCDI III.

Data Availability Statement: Data are contained within the article.

Acknowledgments: The work with the NISA setup at "Ilie Murgulescu" Institute of Physical Chemistry was possible due to the Research Collaboration Agreement between the Romanian Institution and Paul Scherrer Institute, Switzerland. Cristian Iacob from Computer Power SRL, Romania, is acknowledged for providing technical support. Florina Teodorescu from the Institute of Physical Chemistry, Romania, is acknowledged for valuable discussions. The authors are thankful to Marta Ferro from the University of Aveiro, Portugal, for the TEM characterization.

Conflicts of Interest: The authors declare no conflicts of interest.

References

1. Atkins, P.; de Paula, J. *Physical Chemistry*, 8th ed.; W. H. Freeman and Company: New York, NY, USA, 2006.
2. Peng, D.Y.; Robinson, D.B. A New Two-Constant Equation of State. *Ind. Eng. Chem. Fundam.* **1976**, *15*, 59–64. [CrossRef]
3. Wang, S.; Xu, D.; Guo, Y.; Tang, X.; Wang, Y.; Zhang, J.; Ma, H.; Qian, L.; Li, Y. *Supercritical Water Processing Technologies for Environment, Energy and Nanomaterial Applications*; Springer: Singapore, 2020; ISBN 978-981-13-9325-9.
4. Simeoni, G.G.; Bryk, T.; Gorelli, F.A.; Krisch, M.; Ruocco, G.; Santoro, M.; Scopigno, T. The Widom line as the crossover between liquid-like and gas-like behaviour in supercritical fluids. *Nat. Phys.* **2010**, *6*, 503–507. [CrossRef]
5. Simeski, F.; Ihme, M. Supercritical fluids behave as complex networks. *Nat. Commun.* **2023**, *14*, 1996. [CrossRef]
6. Banuti, D.T. Crossing the Widom-line—Supercritical pseudo-boiling. *J. Supercrit. Fluids* **2015**, *98*, 12–16. [CrossRef]
7. Maxim, F.; Contescu, C.; Boillat, P.; Niceno, B.; Karalis, K.; Testino, A.; Ludwig, C. Visualization of supercritical water pseudo-boiling at Widom line crossover. *Nat. Commun.* **2019**, *10*, 4114. [CrossRef] [PubMed]
8. Maxim, F.; Karalis, K.; Boillat, P.; Banuti, D.T.; Marquez Damian, J.I.; Niceno, B.; Ludwig, C. Thermodynamics and Dynamics of Supercritical Water Pseudo-Boiling. *Adv. Sci.* **2021**, *8*, 2002312. [CrossRef] [PubMed]
9. Banuti, D.T.; Raju, M.; Ihme, M. Similarity law for Widom lines and coexistence lines. *Phys. Rev. E* **2017**, *95*, 052120. [CrossRef]

10. de Souza, G.B.M.; Pereira, M.B.; Mourão, L.C.; dos Santos, M.P.; de Oliveira, J.A.; Garde, I.A.A.; Alonso, C.G.; Jegatheesan, V.; Cardozo-Filho, L. Supercritical water technology: An emerging treatment process for contaminated wastewaters and sludge. *Rev. Environ. Sci. Bio/Technol.* **2022**, *21*, 75–104. [CrossRef]
11. Okolie, J.A.; Rana, R.; Nanda, S.; Dalai, A.K.; Kozinski, J.A. Supercritical water gasification of biomass: A state-of-the-art review of process parameters, reaction mechanisms and catalysis. *Sustain. Energy Fuels* **2019**, *3*, 578–598. [CrossRef]
12. Vadillo, V.; Sánchez-Oneto, J.; Portela, J.R.; Martínez de la Ossa, E.J. Supercritical Water Oxidation. In *Advanced Oxidation Processes for Waste Water Treatment*; Elsevier: Amsterdam, The Netherlands, 2018; pp. 333–358, ISBN 9780128105252.
13. Queiroz, A.; Pedroso, G.B.; Kuriyama, S.N.; Fidalgo-Neto, A.A. Subcritical and supercritical water for chemical recycling of plastic waste. *Curr. Opin. Green Sustain. Chem.* **2020**, *25*, 100364. [CrossRef]
14. Vogel, F. Hydrothermal Production of SNG from WET Biomass. In *Synthetic Natural Gas from Coal, Dry Biomass, and Power-to-Gas Applications*; Schildhauer, T.J., Biollaz, S.M.A., Eds.; Wiley: Hoboken, NJ, USA, 2016; pp. 249–278, ISBN 9781119191339.
15. Maxim, F.; Poenaru, I.; Toma, E.E.; Stoian, G.S.; Teodorescu, F.; Hornoiu, C.; Tanasescu, S. Functional Materials for Waste-to-Energy Processes in Supercritical Water. *Energies* **2021**, *14*, 7399. [CrossRef]
16. Xiang, H.; Baudouin, D.; Vogel, F. Metal oxide nanoparticles embedded in porous carbon for sulfur absorption under hydrothermal conditions. *Sci. Rep.* **2023**, *13*, 9987. [CrossRef] [PubMed]
17. Lane, M.K.M.; Zimmerman, J.B. Controlling metal oxide nanoparticle size and shape with supercritical fluid synthesis. *Green Chem.* **2019**, *21*, 3769–3781. [CrossRef]
18. Adschiri, T.; Takami, S.; Umetsu, M.; Ohara, S.; Naka, T.; Minami, K.; Hojo, D.; Togashi, T.; Arita, T.; Taguchi, M.; et al. Supercritical Hydrothermal Reactions for Material Synthesis. *Bull. Chem. Soc. Jpn.* **2023**, *96*, 133–147. [CrossRef]
19. Darr, J.A.; Zhang, J.; Makwana, N.M.; Weng, X. Continuous Hydrothermal Synthesis of Inorganic Nanoparticles: Applications and Future Directions. *Chem. Rev.* **2017**, *117*, 11125–11238. [CrossRef]
20. Sharma, M.; Joshi, M.; Nigam, S.; Shree, S.; Avasthi, D.K.; Adelung, R.; Srivastava, S.K.; Kumar Mishra, Y. ZnO tetrapods and activated carbon based hybrid composite: Adsorbents for enhanced decontamination of hexavalent chromium from aqueous solution. *Chem. Eng. J.* **2019**, *358*, 540–551. [CrossRef]
21. Taha, A.; Ben Aissa, M.; Da'na, E. Green Synthesis of an Activated Carbon-Supported Ag and ZnO Nanocomposite for Photocatalytic Degradation and Its Antibacterial Activities. *Molecules* **2020**, *25*, 1586. [CrossRef] [PubMed]
22. Lakkaboyana, S.K.; Khantong, S.; Asmel, N.K.; Yuzir, A.; Wan Yaacob, W.Z. Synthesis of Copper Oxide Nanowires-Activated Carbon (AC@CuO-NWs) and Applied for Removal Methylene Blue from Aqueous Solution: Kinetics, Isotherms, and Thermodynamics. *J. Inorg. Organomet. Polym. Mater.* **2019**, *29*, 1658–1668. [CrossRef]
23. Schwarz, J.A.; Contescu, C.; Contescu, A. Methods for Preparation of Catalytic Materials. *Chem. Rev.* **1995**, *95*, 477–510. [CrossRef]
24. Román-Martínez, M.C.; Cazorla-Amorós, D.; Linares-Solano, A.; De Lecea, C.S.-M.; Yamashita, H.; Anpo, M. Metal-support interaction in Pt/C catalysts. Influence of the support surface chemistry and the metal precursor. *Carbon N. Y.* **1995**, *33*, 3–13. [CrossRef]
25. Zhang, W.-D. Growth of ZnO nanowires on modified well-aligned carbon nanotube arrays. *Nanotechnology* **2006**, *17*, 1036–1040. [CrossRef]
26. Chang, J.-Y.; Mai, F.-D.; Lo, B.; Chang, J.-J.; Tzing, S.-H.; Ghule, A.; Ling, Y.-C. Transportation of silver nanopaticles in nanochannels of carbon nanotubes with supercritical water. *Chem. Commun.* **2003**, *18*, 2362–2363. [CrossRef]
27. Munnik, P.; de Jongh, P.E.; de Jong, K.P. Recent Developments in the Synthesis of Supported Catalysts. *Chem. Rev.* **2015**, *115*, 6687–6718. [CrossRef]
28. Otsu, J.; Oshima, Y. New approaches to the preparation of metal or metal oxide particles on the surface of porous materials using supercritical water: Development of supercritical water impregnation method. *J. Supercrit. Fluids* **2005**, *33*, 61–67. [CrossRef]
29. Qiu, B.; Han, L.; Wang, J.; Chang, L.; Bao, W. Preparation of Sorbents Loaded on Activated Carbon to Remove H 2 S from Hot Coal Gas by Supercritical Water Impregnation. *Energy Fuels* **2011**, *25*, 591–595. [CrossRef]
30. Kumar, K.Y.; Muralidhara, H.B.; Nayaka, Y.A.; Hanumanthappa, H.; Veena, M.S.; Kumar, S.R.K. Hydrothermal Synthesis of Hierarchical Copper Oxide Nanoparticles and its Potential Application as Adsorbent for Pb(II) with High Removal Capacity. *Sep. Sci. Technol.* **2014**, *49*, 2389–2399. [CrossRef]
31. Ates, A.; Hatipoglu, H. Evaluation of Stability and Catalytic Activity in Supercritical Water of Zinc Oxide Samples Prepared by the Sol–Gel Method. *J. Inorg. Organomet. Polym. Mater.* **2021**, *31*, 4581–4593. [CrossRef]
32. Fatima, R.; Warsi, M.F.; Zulfiqar, S.; Ragab, S.A.; Shakir, I.; Sarwar, M.I. Nanocrystalline transition metal oxides and their composites with reduced graphene oxide and carbon nanotubes for photocatalytic applications. *Ceram. Int.* **2020**, *46*, 16480–16492. [CrossRef]
33. Farooq, S.; Al Maani, A.H.; Naureen, Z.; Hussain, J.; Siddiqa, A.; Al Harrasi, A. Synthesis and characterization of copper oxide-loaded activated carbon nanocomposite: Adsorption of methylene blue, kinetic, isotherm, and thermodynamic study. *J. Water Process Eng.* **2022**, *47*, 102692. [CrossRef]
34. Azam, A.; Ahmed, A.S.; Oves, M.; Khan, M.S.; Memic, A. Size-dependent antimicrobial properties of CuO nanoparticles against Gram-positive and -negative bacterial strains. *Int. J. Nanomed.* **2012**, *7*, 3527–3535. [CrossRef]
35. Karalis, K.; Ludwig, C.; Niceno, B. Supercritical water anomalies in the vicinity of the Widom line. *Sci. Rep.* **2019**, *9*, 15731. [CrossRef] [PubMed]

36. Ludwig, C.; Casey, W.H. On the Mechanisms of Dissolution of Bunsenite [NiO(s)] and Other Simple Oxide Minerals. *J. Colloid Interface Sci.* **1996**, *178*, 176–185. [CrossRef]
37. Sawai, O.; Oshima, Y. Mechanism of silver nano-particles formation on α-alumina using supercritical water. *J. Mater. Sci.* **2008**, *43*, 2293–2299. [CrossRef]
38. Barroso-Bogeat, A.; Alexandre-Franco, M.; Fernández-González, C.; Gómez-Serrano, V. Activated carbon surface chemistry: Changes upon impregnation with Al(III), Fe(III) and Zn(II)-metal oxide catalyst precursors from NO^{3-} aqueous solutions. *Arab. J. Chem.* **2019**, *12*, 3963–3976. [CrossRef]
39. Martin, R.B. A stability ruler for metal ion complexes. *J. Chem. Educ.* **1987**, *64*, 402. [CrossRef]
40. Santoso, S.P.; Angkawijaya, A.E.; Ju, Y.-H. Complex stability in aqueous solution of metal ions (Cu^{2+}, Zn^{2+}, and Mn^{2+}) with pyrocatechuic acid ligand. *Int. J. Adv. Sci. Eng. Technol.* **2015**, *3*, 23–28.
41. Irving, H.; Williams, R.J.P. The stability of transition-metal complexes. *J. Chem. Soc.* **1953**, 3192–3210. [CrossRef]
42. Kwon, B.; Liebenberg, L.; Jacobi, A.M.; King, W.P. Heat transfer enhancement of internal laminar flows using additively manufactured static mixers. *Int. J. Heat Mass Transf.* **2019**, *137*, 292–300. [CrossRef]
43. Yoko, A.; Seong, G.; Tomai, T.; Adschiri, T. Continuous flow synthesis of nanoparticles using supercritical water: Process design, surface control, and nanohybrid materials. *KONA Powder Part. J.* **2020**, *37*, 28–41. [CrossRef]
44. Demoisson, F.; Ariane, M.; Leybros, A.; Muhr, H.; Bernard, F. Design of a reactor operating in supercritical water conditions using CFD simulations. Examples of synthesized nanomaterials. *J. Supercrit. Fluids* **2011**, *58*, 371–377. [CrossRef]
45. Zhou, L.; Wang, S.Z.; Xu, D.H.; Guo, Y. Impact of Mixing for the Production of CuO Nanoparticles in Supercritical Hydrothermal Synthesis. *Ind. Eng. Chem. Res.* **2014**, *53*, 481–493. [CrossRef]
46. Baruah, S.; Dutta, J. Hydrothermal growth of ZnO nanostructures. *Sci. Technol. Adv. Mater.* **2009**, *10*, 013001. [CrossRef] [PubMed]
47. Demoisson, F.; Piolet, R.; Ariane, M.; Leybros, A.; Bernard, F. Influence of the pH on the ZnO nanoparticle growth in supercritical water: Experimental and simulation approaches. *J. Supercrit. Fluids* **2014**, *95*, 75–83. [CrossRef]
48. Aboelfetoh, E.F.; Elhelaly, A.A.; Gemeay, A.H. Synergistic effect of Cu(II) in the one-pot synthesis of reduced graphene oxide (rGO/CuxO) nanohybrids as adsorbents for cationic and anionic dyes. *J. Environ. Chem. Eng.* **2018**, *6*, 623–634. [CrossRef]